Measurement of a Photoinduced Transition from a Nonordered Phase to a Transient Ordered Phase in the Organic Quantum-Paraelectric Compound dimethyltetrathiafulvalene-dibromodichloro-*p*-benzoquinone Using Femtosecond Laser Irradiation

Tatsuya Miyamoto,[1] Kazuki Kimura,[1] Takanori Hamamoto,[1] Hirotaka Uemura,[1] Hiroyuki Yada,[1] Hiroyuki Matsuzaki,[2] Sachio Horiuchi,[2,3] and Hiroshi Okamoto[1]

[1]*Department of Advanced Materials Science, University of Tokyo, Kashiwa, Chiba 277-8561, Japan*
[2]*National Institute of Advanced Industrial Science and Technology (AIST), Tsukuba, Ibaraki 305-8562, Japan*
[3]*CREST, Japan Science and Technology Agency, Chiyoda-ku, Tokyo 102-0076, Japan*

(Received 1 March 2013; revised manuscript received 2 August 2013; published 29 October 2013)

We report a new photoinduced transition from a nonordered phase to a transient ordered phase with symmetry breaking in an organic charge-transfer compound, dimethyltetrathiafulvalene (DMTTF)-dibromodichloro-*p*-benzoquinone (2, 6QBr$_2$Cl$_2$), which is a neutral compound located near the neutral-ionic phase boundary and shows quantum paraelectricity at low temperatures. By an irradiation of a femtosecond laser pulse, an ionic domain consisting of ~40 molecules is introduced into the neutral lattice per photon, giving rise to coherent molecular oscillations with fractional charge modulations over ~400 molecules. This response is due to the recovery of ferroelectric nature from the quantum paraelectricity by a photoinjection of an ionic domain with a large dipole moment.

DOI: 10.1103/PhysRevLett.111.187801 PACS numbers: 78.30.Jw, 77.80.−e, 78.20.−e, 78.47.jg

A material located near a boundary between two competing phases often exhibits a rapid change in electronic structure through photoirradiation. This phenomenon, a photoinduced phase transition (PIPT), is important for future optical-switching or memory devices [1]. In most photoinduced phase transitions, an ordered phase is destabilized by photoirradiation and a nonordered phase appears. A typical example is the photoinduced collapse of a Mott gap and the subsequent appearance of a metallic state as observed in one-dimensional (1D) Mott insulators of bromine-bridged Ni-chain compounds [2] and organic bis(ethylenedithio)tetrathiafulvalene-difluorotetracyanoquinodimethane solids [3], and 2D Mott insulators of undoped cuprates [4]. Photoinduced meltings of the charge-order states in perovskite manganites [5] and organic molecular compounds [6], the Peierls state in VO_2 [7,8], charge-density-wave states in 1T-TaS_2 [9], $TbTe_3$ [10,11], and $K_{0.3}MoO_3$ [12], and the spin-Peierls phase in alkali-metal tetracyanoquinodimethane salts [13] are other well-known examples. In general, however, generating an ordered phase with a lower symmetry or equivalently giving rise to a symmetry breaking through photoirradiation is difficult and only a few examples have been reported [14]. In order to realize a transition with symmetry breaking using light, we focus on quantum paraelectricity (QP). In materials with QP, ferroelectric orders are destabilized due to quantum lattice fluctuations at low temperatures. In the typical quantum-paraelectric material, $SrTiO_3$, *A*-site cation exchange gives rise to ferroelectricity through the enhancement of dipole interactions [15]. If photoirradiation creates large dipole moments in materials with quantum paraelectricity, the instability to ferroelectricity might revive. In $SrTiO_3$, photoirradiation generates electron and hole carriers, so that ferroelectricity could not be restored [16,17]. The material studied here is an organic charge-transfer (CT) compound, 4,4'-dimethyltetrathiafulvalene(DMTTF) -3,5-dibromo-2,6-dichloro-*p*-benzoquinone(2, 6QBr$_2$Cl$_2$) with QP at low temperatures [18].

In DMTTF-QBr$_n$Cl$_{4-n}$ [Fig. 1(a)], donor (*D*) (DMTTF) and acceptor (*A*) molecules (QBr$_n$Cl$_{4-n}$) arrange in

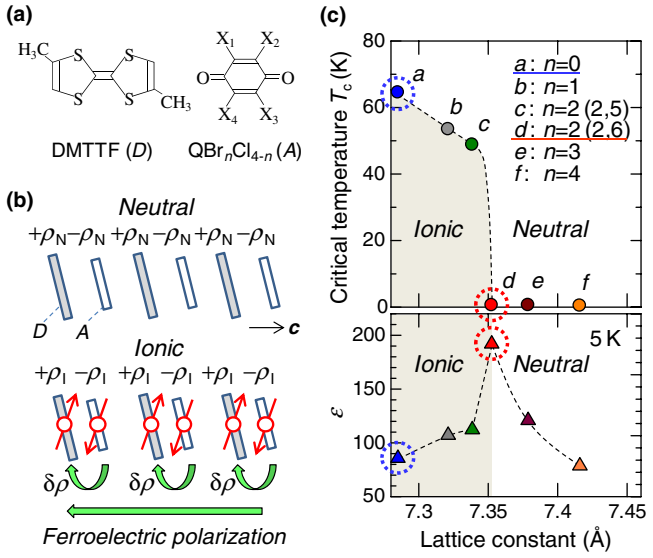

FIG. 1 (color online). (a) Molecular structures of DMTTF and QBr$_n$Cl$_{4-n}$. (b) Schematic of *NI* transitions and the formation of the ferroelectric polarization. (c) Phase diagram of *NI* transitions in DMTTF-QBr$_n$Cl$_{4-n}$ and dielectric constant ε (30 kHz) at 5 K showing the criticality of DMTTF-2, 6QBr$_2$Cl$_2$ ($n = 2$).

alternate DA stacks along the c axis [Fig. 1(b)] [19]. DMTTF-QCl$_4$(CA) shows a neutral (N) to ionic (I) transition at $T_c = 65$ K from $(\cdots D^{+0.3}A^{-0.3}D^{+0.3}A^{-0.3}\cdots)$ to $(\cdots D^{+0.5}A^{-0.5}D^{+0.5}A^{-0.5}\cdots)$ [18,20]. This is a second-order or very weak first-order phase transition [21,22], contrary to the strong first-order phase transition of TTF-CA, a typical material showing the NI transition [23]. The I phase is stabilized by the increase in the Madelung potential due to a contraction of the lattice at low temperatures. In the I phase, DA molecules dimerize due to the spin-Peierls mechanism. Moreover, the phases of dimeric displacements are two-dimensionally ordered in the ac plane, showing a ferroelectric nature [18]. The ferroelectric ac planes arrange antiferroelectrically along the b axis, resulting in the disappearance of macroscopic polarization. By substituting Cl with Br in QCl$_4$, a unique phase diagram was obtained [Fig. 1(c)]. With the increase of n, the Madelung potential decreases with the increase of the c-axis lattice constant, and T_c decreases. For $n \geq 3$, the transition disappears. In DMTTF-2, 6QBr$_2$Cl$_2$, the dielectric constant ε monotonically increases with decreasing temperature and becomes constant below 20 K [see Fig. 5(a)]. This behavior is characteristic of QP. ε values at 5 K are plotted versus lattice constant in Fig. 1(c) [18,20], showing criticality in DMTTF-2, 6QBr$_2$Cl$_2$. In order to clarify the photoresponse characteristic of QP, we performed comparative studies on DMTTF-2, 6QBr$_2$Cl$_2$ and DMTTF-QCl$_4$, which we express hereafter as $n = 2$ and $n = 0$, respectively.

Single crystals of $n = 0$ and $n = 2$ were prepared following the method previously reported [18]. All the optical measurements were performed on the ac plane. Polarized Raman spectra were measured using a Raman spectrometer equipped with a He-Ne laser (1.96 eV) and an optical microscope. For pump-probe measurements, we used a Ti:Al_2O_3 regenerative amplifier as a light source (1.57 eV, pulse width of 130 fs, and repetition rate of 1 kHz). The output from the regenerative amplifier was divided into two beams, which were used as excitation sources for two optical parametric amplifiers (OPAs). From two OPAs, pump (0.65 eV) and probe (2.0–2.5 eV) pulses were obtained. The delay time t_d of the probe pulse relative to the pump pulse was controlled by changing the path length of the pump pulse. The temporal resolution of the system was ~180 fs. The excitation photon density x_{ph} was defined by the photon density per unit volume within the absorption depth and evaluated by $x_{ph} = (1 - 1/e) \times (1 - R_p)I_p/l_p$, where I_p, l_p, R_p, and e are the excitation photon density per unit area, the absorption depth, the reflection loss of the pump light, and Napier's constant, respectively.

Figures 2(a) and 2(b) shows the reflectivity (R) spectra at 12 K (I phase) and 75 K (N phase) in $n = 0$ and at 12 K (quantum paraelectric N phase) in $n = 2$, respectively. Strong bands at ~0.6 eV polarized along the c axis are CT transitions between D and A molecules. The bands at

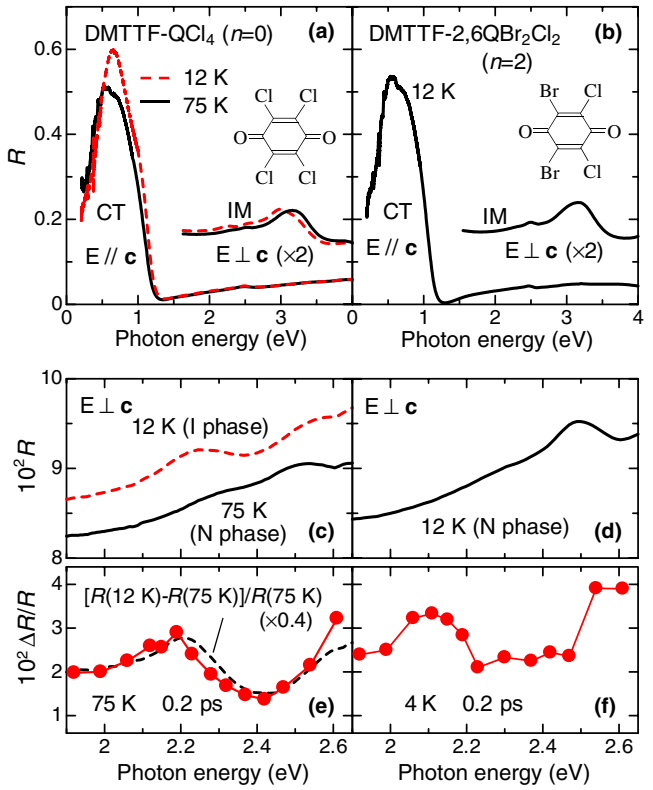

FIG. 2 (color online). Reflectivity (R) spectra of (a) DMTTF-QCl$_4$ ($n = 0$) and (b) DMTTF-2, 6QBr$_2$Cl$_2$ ($n = 2$). (c) and (d) are the expanded R spectra. Photoinduced R change ($\Delta R/R$) spectra just after the photoirradiation in (e) $n = 0$ and (f) $n = 2$. The broken line in (e) is the differential reflectivity spectrum $[R(12\text{ K}) - R(75\text{ K})]/R(75\text{ K})$ between the I phase (12 K) and N phase (75 K) in $n = 0$.

2.25 eV and 2.5 eV shown in Figs. 2(c) and 2(d) polarized perpendicular to c are due to intramolecular transitions of DMTTF and QBr$_n$Cl$_{4-n}$, respectively [24]. In order to detect changes in the molecular ionicity ρ, we focus on the intramolecular transition of DMTTF, since its spectral shape and intensity depend sensitively on ρ [25,26].

Photoinduced reflectivity changes $\Delta R/R$ at 75 K in $n = 0$ and at 4 K in $n = 2$ are shown in Figs. 2(e) and 2(f), respectively. Pump and probe light are polarized parallel and perpendicular to the stacking axis c, respectively. The excitation photon density x_{ph} is 0.021 (0.027) ph/DA in $n = 0$ ($n = 2$). The broken line in Fig. 2(e) is $[R(12\text{ K}) - R(75\text{ K})]/R(75\text{ K}) \equiv \Delta R_{NI}/R$, which is the spectral change expected when N states are converted to I states. The $\Delta R/R$ spectrum in $n = 0$ is in good agreement with $\Delta R_{NI}/R$, demonstrating that a photoinduced NI transition occurs. $\Delta R/R$ at 4 K in $n = 2$ [Fig. 2(f)] exhibited nearly the same spectral change as in $n = 0$, suggesting that a similar NI conversion is induced.

In Figs. 3(a) and 3(b), we show x_{ph} dependence of the maximum values ($\Delta R_M/R$) in the time evolutions of $\Delta R/R$ at ~0.2 ps as circles [see Figs. 4(a) and 4(b)], which are almost proportional to x_{ph}. In $n = 0$, it was deduced from

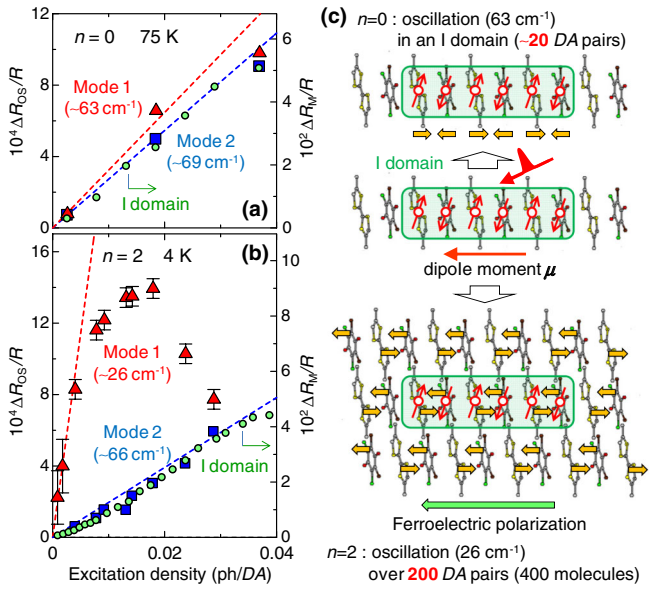

FIG. 3 (color online). Excitation density (x_{ph}) dependence of oscillation amplitudes ($\Delta R_{OS}/R$) and maximum values ($\Delta R_M/R$) of reflectivity changes (circles) reflecting photogenerated I domains; (a) $n = 0$ (75 K, 2.2 eV probe) and (b) $n = 2$ (4 K, 2.1 eV probe). Broken lines show linear relations. (c) Schematics of coherent oscillations in $n = 0$ (upper) and $n = 2$ (lower). In $n = 2$, coherent oscillations are generated not only in an I domain with ~20 DA pairs but also in surrounding wide regions over ~400 molecules.

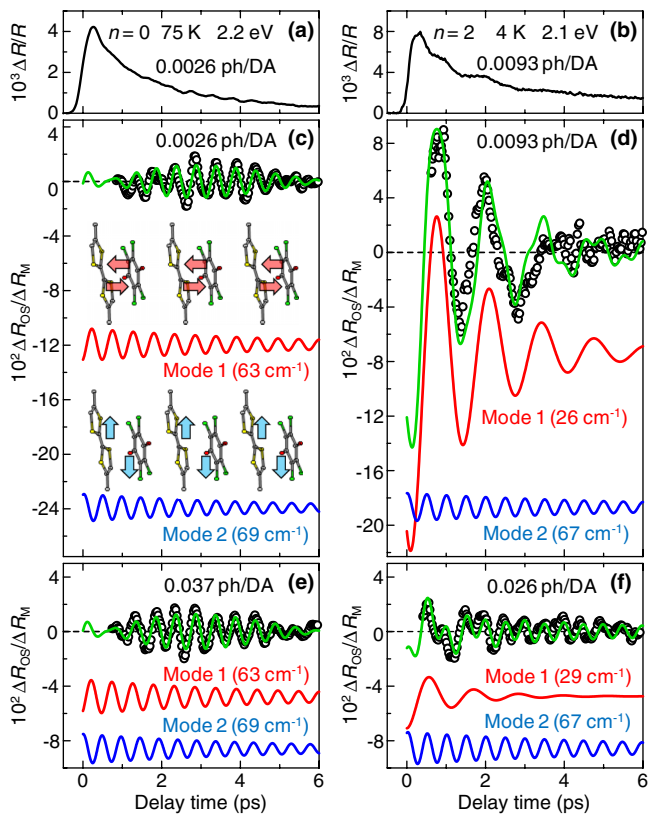

FIG. 4 (color online). Time characteristics of $\Delta R/R$ reflecting photogenerated I states in (a) $n = 0$ at 75 K and (b) $n = 2$ at 4 K. Oscillatory components ΔR_{OS} (open circles) normalized by the maximum values ΔR_M of reflectivity changes in $n = 0$ and $n = 2$ for the weak (c),(d) and strong (e),(h) excitation densities (x_{ph}). Green lines show calculated curves and the other lines show constituent oscillatory components. Modes 1 and 2 are illustrated in (c).

the magnitudes of $\Delta R/R(= 0.4 \times \Delta R_{NI}/R)$ and x_{ph} (0.021 ph/DA) [Fig. 2(e)] that about 20 DA pairs are ionized per photon and microscopic I domains are formed [the middle panel of Fig. 3(c)]. Such an I domain formation in neutral CT compounds near the NI phase boundary was demonstrated by previous experimental [27–29] and theoretical studies [30–32]. $n = 2$ exhibited nearly the same signal magnitudes [Fig. 2(f)] [33], suggesting that the NI conversion efficiency is comparable with $n = 0$.

Figures 4(a) and 4(b) show the time characteristics of the $\Delta R/R$ peaks at around 2 eV measured with small x_{ph} (< 0.01 ph/DA) in the two compounds, which decay in several picoseconds in common. The characteristic response of $n = 2$ manifests itself in oscillations of $\Delta R/R$. By subtracting the background rise and decay from $\Delta R/R$, we extracted the oscillatory components ΔR_{OS} and show these, normalized by ΔR_M, in Figs. 4(c)–4(f).

In $n = 0$, $\Delta R_{OS}/\Delta R_M$ can be well reproduced by the sum of two damped oscillations, mode 1 with 63 cm^{-1} and mode 2 with 69 cm^{-1} [Fig. 4(c)]. The oscillations are of the cosine type, indicating a displacive excitation of coherent phonons [34]. Similar oscillations were observed in the photoinduced NI transition of TTF-CA and assigned to the dimeric lattice mode in I domains driven by the spin-Peierls mechanism [27–29]. Taking the Raman spectroscopic studies into account, we could assign modes 1 and 2 to the lattice modes with dimeric displacements [35] along the molecular stacks (longitudinal dimeric mode) and along the molecular planes (shear-type dimeric mode), respectively, which are illustrated in Fig. 4(c). Further details are reported in the Supplemental Material S1–S3 [36]. Oscillatory profiles were independent of x_{ph} [Figs. 4(c) and 4(e)], and the x_{ph} dependence of the oscillation amplitudes was similar to $\Delta R_M/R$ [Fig. 3(a)]. This suggests that oscillations are generated in an I domain as illustrated in Fig. 3(c) (upper panel).

Oscillatory components in $n = 2$ were also almost reproduced by the sum of two cosine-type oscillations with ~26 cm^{-1} and ~67 cm^{-1} [Fig. 4(d)], which could be assigned to longitudinal and shear-type dimeric modes and therefore labeled as modes 1 and 2, respectively (see Supplemental Material S4 and S5 [36]). Mode 1 has a large amplitude compared to mode 2 for $x_{ph} = 0.0093$ ph/DA; normalized amplitude $\Delta R_{OS}/\Delta R_M$ of mode 1 is ~2.5% in $n = 0$ [Fig. 4(c)], but reaches ~25% in $n = 2$ [Fig. 4(d)]. When x_{ph} was increased up to 0.026 ph/DA, the normalized amplitude $\Delta R_{OS}/\Delta R_M$ of mode 1 was considerably decreased, while that of mode 2 was almost unchanged [Fig. 4(f)]. The x_{ph} dependence of oscillation amplitudes

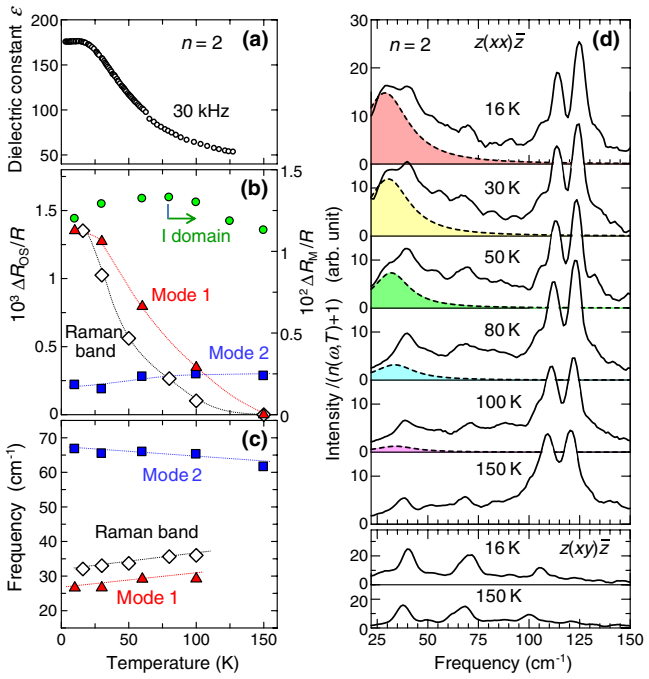

FIG. 5 (color online). (a) Temperature dependence of dielectric constant at 30 kHz in $n = 2$ [18]. (b) Temperature dependence of the oscillation amplitudes $\Delta R_{OS}/R$ and the maximum values of reflectivity changes $\Delta R_M/R$ reflecting the I domain size [36]. Diamonds show the integrated intensity of the Raman band [broken lines in (d)] reflecting the magnitude of fluctuating dimerizations [36]. (c) Temperature dependences of the frequencies of the oscillation modes (1 and 2) and the Raman band shown by broken lines in (d). (d) Polarized Raman spectra.

$\Delta R_{OS}/R$ [Fig. 3(b)] shows that mode 1 is saturated at very low excitation density ($x_s \sim 0.005$ ph/DA). This saturation behavior is not due to the heating of the system as detailed in the Supplemental Material S6 [36]. It is attributable to space filling of the oscillating region. Assuming the space filling, we can consider that oscillation mode 1 is generated over $1/x_s \sim 200$ DA pairs (400 molecules). Since the size of an I domain is ~20 DA pairs, the oscillations should be generated not only within an I domain but also in the surrounding wide region. This phenomenon is illustrated in Fig. 3(c) (lower panel).

In order to clarify the interrelation between coherent oscillations and QP, we investigated the temperature dependence of the oscillations in $n = 2$. Their amplitudes and frequencies were plotted in Figs. 5(b) and 5(c), respectively (see Supplemental Material S5 [36]). Although $\Delta R_M/R$ is independent of temperature, the amplitude of mode 1 shows a prominent increase with decreasing temperature, which corresponds well to the enhancement of ε shown in Fig. 5(a). This indicates a strong correlation of mode 1 with QP. In contrast, mode 2 does not show significant temperature dependence.

The temperature dependence of the polarized Raman spectra for $z(xx)\bar{z}$ and $z(xy)\bar{z}$, shown in Fig. 5(d), gives important information about low-temperature lattice dynamics associated with QP. Here, x corresponds to c and z denotes the direction of the incident light normal to the crystal surface. The band at ~30 cm^{-1} [broken lines in Fig. 5(d)] activated for $z(xx)\bar{z}$ gains the intensity and shifts to lower frequency with decreasing temperature [Figs. 5(b) and 5(c)]. Such behaviors would be characteristic of QP. This band could be assigned to the longitudinal dimeric mode activated by fluctuating dimerizations (see Supplemental Material S4 [36]). Oscillation mode 1 shows a similar temperature dependence (triangles in the same figures), indicating again its strong correlation with QP.

Now, we can discuss the mechanism for the enhancements of oscillation mode 1. At low temperatures, dimeric molecular displacements occur along c, while their phases are random in time and space due to quantum fluctuations. By a photoinjection of an I domain, two coherent oscillations are generated by the spin-Peierls mechanism. The large dipole moment of an I domain restores the instability to ferroelectricity, so that in-phase dimeric displacements along c and subsequent coherent oscillation (mode 1) are induced not only within the I domain but also in the surrounding wide region over ~400 molecules. In other words, by a photoinjection of an I domain, ferroelectric nature disrupted by quantum fluctuations is recovered and phases of fluctuating dimerizations are locked. In this way, photoinjection results in large coherent oscillations. The directions of dipole moments of photogenerated I domains can be right or left, so that destructive interference of coherent oscillations caused by I domains initially generated in different stacks occur when x_{ph} increases. This is the reason for the saturation of the oscillation at small x_{ph} and the subsequent decrease of the oscillation in Fig. 3(b) (triangles).

It is valuable to comment on the direction and magnitude of the polarization induced by dimeric molecular displacements. According to the point charge model, in which charges are set on the center of gravity in each molecule, a direction of a polarization induced by the dimeric molecular displacements is parallel (antiparallel) to the direction of the molecular displacements of D (A) molecules. In this model, the direction of the dimerization-induced polarization $\boldsymbol{P}$ does not accord with the direction of the dipole moment $\boldsymbol{\mu}$ within a 1D I domain discussed above, so that the photogenearation of a 1D I domain never restores ferroelectricity. The recent x-ray diffraction [37] and theoretical studies [38,39] on a typical NI transition material, TTF-CA, revealed that the ferroelectric polarization $\boldsymbol{P}$ directs antiparallel (parallel) to the displacements of D (A) molecules, opposite to the simple expectation from the point charge model. This suggests that the ferroelectric polarization in the I phase is governed by the intradimer fractional CTs, $\delta\rho$, as shown in Fig. 1(b), and the ferroelectricity has an electronic origin. In the ac planes of $n = 0$ and $n = 2$, a similar ferroelectric mechanism can also be considered. When the coherent oscillation is generated over ~200 DA pairs around a 1D I domain with 20 DA pairs, the magnitude of the additional CT from A to D

molecule by the initial dimeric molecular displacements was evaluated to be 0.003, which is almost equal to 1% of the degree of CT ($\rho \sim 0.3$) in the N phase (see Supplemental Material S7 [36]).

In summary, we demonstrated in a molecular compound that ferroelectric nature disrupted by quantum fluctuations was restored by a photoinduced ionic domain with a large dipole moment. This phenomenon can be considered as a transient version of ferroelectricity revived by an injection of a dipole moment as observed in the substitution effect in $SrTiO_3$. This discovery represents a new method to induce a photoinduced phase transition with a symmetry breaking in solid. Furthermore, our results present new aspects of neutral-ionic transitions; dimeric molecular displacements can occur even in the neutral lattice, which demonstrates that electrostatic or dipole interactions play an important role in molecular dimerizations.

This work was supported in part by a Grant-in-Aid by MEXT (No. 20110005 and No. 20110003).

[1] S. Iwai and H. Okamoto, J. Phys. Soc. Jpn. **75**, 011007 (2006).
[2] S. Iwai, M. Ono, A. Maeda, H. Matsuzaki, H. Kishida, H. Okamoto, and Y. Tokura, Phys. Rev. Lett. **91**, 057401 (2003).
[3] H. Okamoto, H. Matsuzaki, T. Wakabayashi, Y. Takahashi, and T. Hasegawa, Phys. Rev. Lett. **98**, 037401 (2007).
[4] H. Okamoto, T. Miyagoe, K. Kobayashi, H. Uemura, H. Nishioka, H. Matsuzaki, A. Sawa, and Y. Tokura, Phys. Rev. B **83**, 125102 (2011).
[5] M. Fiebig, K. Miyano, Y. Tomioka, and Y. Tokura, Science **280**, 1925 (1998).
[6] M. Chollet, L. Guerin, N. Uchida, S. Fukaya, H. Shimoda, T. Ishikawa, K. Matsuda, T. Hasegawa, A. Ota, H. Yamochi, G. Saito, R. Tazaki, A. Adachi, and S. Koshihara, Science **307**, 86 (2005).
[7] A. Cavalleri, Cs. Tóth, C. W. Siders, J. A. Squier, F. Raksi, P. Forget, and J. C. Kieffer, Phys. Rev. Lett. **87**, 237401 (2001).
[8] C. Kübler, H. Ehrke, R. Huber, R. Lopez, A. Halabica, R. F. Haglund, Jr., and A. Leitenstorfer, Phys. Rev. Lett. **99**, 116401 (2007).
[9] L. Perfetti, P. A. Loukakos, M. Lisowski, U. Bovensiepen, H. Berger, S. Biermann, P. S. Cornaglia, A. Georges, and M. Wolf, Phys. Rev. Lett. **97**, 067402 (2006).
[10] F. Schmitt, P. S. Kirchmann, U. Bovensiepen, R. G. Moore, L. Rettig, M. Krenz, J. H. Chu, N. Ru, L. Perfetti, D. H. Lu, M. Wolf, I. R. Fisher, and Z. X. Shen, Science **321**, 1649 (2008).
[11] R. Yusupov, T. Mertelj, V. V. Kabanov, S. Brazovskii, P. Kusar, J. Chu, I. R. Fisher, and D. Mihailovic, Nat. Phys. **6**, 681 (2010).
[12] A. Tomeljak, H. Schäfer, D. Städter, M. Beyer, K. Biljakovic, and J. Demsar, Phys. Rev. Lett. **102**, 066404 (2009).
[13] H. Okamoto, K. Ikegami, T. Wakabayashi, Y. Ishige, J. Togo, H. Kishida, and H. Matsuzaki, Phys. Rev. Lett. **96**, 037405 (2006).
[14] D. Fausti, O. V. Misochko, and P. H. M. van Loosdrecht, Phys. Rev. B **80**, 161207(R) (2009).
[15] J. G. Bednorz and K. A. Müller, Phys. Rev. Lett. **52**, 2289 (1984).
[16] M. Takesada, T. Yagi, M. Itoh, and S. Koshihara, J. Phys. Soc. Jpn. **72**, 37 (2003).
[17] T. Hasegawa, S. Mouri, Y. Yamada, and K. Tanaka, J. Phys. Soc. Jpn. **72**, 41 (2003).
[18] S. Horiuchi, Y. Okimoto, R. Kumai, and Y. Tokura, J. Am. Chem. Soc. **123**, 665 (2001).
[19] In DMTTF-QBr_nCl_{4-n}, the crystallographic axes change across the NI transition. In this paper, we always use the axes as defined in the high temperature phase in order to avoid confusion.
[20] S. Horiuchi, Y. Okimoto, R. Kumai, and Y. Tokura, Science **299**, 229 (2003).
[21] E. Collet, M. Buron-Le Cointe, M. H. Lemée-Cailleau, I. Toupet, M. Meven, S. Mattauch, G. Heger, and N. Karl, Phys. Rev. B **63**, 054105 (2001).
[22] P. Ranzieri, M. Masino, A. Girlando, and M. H. Lemée-Cailleau, Phys. Rev. B **76**, 134115 (2007).
[23] M. Le Cointe, M. H. Lemée-Cailleau, H. Cailleau, B. Toudic, L. Toupet, G. Heger, F. Moussa, P. Schweiss, K. H. Kraft, and N. Karl, Phys. Rev. B **51**, 3374 (1995).
[24] J. B. Torrance, J. E. Vazquez, J. J. Mayerle, and V. Y. Lee, Phys. Rev. Lett. **46**, 253 (1981).
[25] J. B. Torrance, A. Girlando, J. J. Mayerle, J. I. Crowley, V. Y. Lee, P. Batail, and S. J. LaPlaca, Phys. Rev. Lett. **47**, 1747 (1981).
[26] S. Koshihara, Y. Tokura, T. Mitani, G. Saito, and T. Koda, Phys. Rev. B **42**, 6853 (1990).
[27] H. Okamoto, Y. Ishige, S. Tanaka, H. Kishida, S. Iwai, and Y. Tokura, Phys. Rev. B **70**, 165202 (2004).
[28] S. Iwai, Y. Ishige, S. Tanaka, Y. Okimoto, Y. Tokura, and H. Okamoto, Phys. Rev. Lett. **96**, 057403 (2006).
[29] H. Uemura and H. Okamoto, Phys. Rev. Lett. **105**, 258302 (2010).
[30] N. Nagaosa and J. Takimoto, J. Phys. Soc. Jpn. **55**, 2745 (1986).
[31] K. Yonemitsu, J. Phys. Soc. Jpn. **73**, 2879 (2004).
[32] K. Iwano, Phys. Rev. Lett. **97**, 226404 (2006).
[33] The magnitude of the signal is $\Delta R_M/R \sim 3.4 \times 10^{-2}$ for 0.027 ph/DA in $n = 0$ and $\Delta R_M/R \sim 2.9 \times 10^{-2}$ for 0.021 ph/DA in $n = 2$.
[34] H. J. Zeiger, J. Vidal, T. K. Cheng, E. P. Ippen, G. Dresselhaus, and M. S. Dresselhaus, Phys. Rev. B **45**, 768 (1992).
[35] G. D' Avino, M. Masino, A. Girlando, and A. Painelli, Phys. Rev. B **83**, 161105 (2011).
[36] See Supplemental Material at http://link.aps.org/supplemental/10.1103/PhysRevLett.111.187801 for the details of dimeric molecular displacements, polarized Raman Spectra, and coherent oscillations.
[37] K. Kobayashi, S. Horiuchi, R. Kumai, F. Kagawa, Y. Murakami, and Y. Tokura, Phys. Rev. Lett. **108**, 237601 (2012).
[38] G. Giovannetti, S. Kumar, A. Stroppa, J. van den Brink, and S. Picozzi, Phys. Rev. Lett. **103**, 266401 (2009).
[39] S. Ishibashi and K. Terakura, Physica (Amsterdam) **405**, S338 (2010).